

NLTE ANALYSIS OF HIGH RESOLUTION *H*-BAND SPECTRA. I. NEUTRAL SILICON*

JUNBO ZHANG^{1,2}, JIANRONG SHI^{1,2}, KAIKE PAN³, CARLOS ALLENDE PRIETO^{4,5}, CHAO LIU¹

¹ Key Laboratory of Optical Astronomy, National Astronomical Observatories, Chinese Academy of Sciences, A20 Datun Road, Chaoyang District, Beijing 100012, China

² School of Astronomy and Space Science, University of Chinese Academy of Sciences, Beijing 100049, China

³ Apache Point Observatory and New Mexico State University, P.O. Box 59, Sunspot, NM, 88349-0059, USA

⁴ Instituto de Astrofísica de Canarias, 38205 La Laguna, Tenerife, Spain and

⁵ Departamento de Astrofísica, Universidad de La Laguna, 38206 La Laguna, Tenerife, Spain

Accepted by ApJ for publication

ABSTRACT

We investigated the reliability of our silicon atomic model and the influence of non-local thermodynamical equilibrium (NLTE) on the formation of neutral silicon (Si I) lines in the near-infrared (near-IR) *H*-band. We derived the differential Si abundances for 13 sample stars with high-resolution *H*-band spectra from the Apache Point Observatory Galactic Evolution Experiment (APOGEE), as well as from optical spectra, both under local thermodynamical equilibrium (LTE) and NLTE conditions. We found that the differences between the Si abundances derived from the *H*-band and from optical lines for the same stars are less than 0.1 dex when the NLTE effects included, and that NLTE reduces the line-to-line scatter in the *H*-band spectra for most sample stars. These results suggest that our Si atomic model is appropriate for studying the formation of *H*-band Si lines. Our calculations show that the NLTE corrections of the Si I *H*-band lines are negative, i.e. the final Si abundances will be overestimated in LTE. The corrections for strong lines depend on surface gravity, and tend to be larger for giants, reaching ~ -0.2 dex in our sample, and up to ~ -0.4 dex in extreme cases of APOGEE targets. Thus, the NLTE effects should be included in deriving silicon abundances from *H*-band Si I lines, especially for the cases where only strong lines are available.

Subject headings: stars: abundances — stars: atmospheres — line: formation — line: profiles

1. INTRODUCTION

Silicon is an important α -element mainly produced during oxygen and neon burning, and returned to the interstellar medium by Type-II Supernovae (SNe II; Woosley & Weaver 1995). SNe Ia may also produce small fraction (Tsujiimoto et al. 1995). Silicon is an important element of the interstellar dust, one of the main electron contributors (only next to Fe and Mg) in the atmospheres of late-type stars (Holweber 1973; Wedemeyer 2001). Silicon abundance is often used as a tracer to explore the formation and evolution of the Solar System (Johnson et al. 2011; Zambardi et al. 2013); and to study the Galactic structure, chemical enrichment history and the origin of the Galaxy in many studies. For example, the silicon abundance, combined with other α -elements, is often adopted as an indicator to distinguish stars from different populations, namely thick- and thin-disks (Lee et al. 2011). A series of studies, e.g. Bensby et al. (2005, 2014); Reddy et al. (2003, 2006); Nissen & Schuster (2010); Zhang et al. (2011) have observed amounts of high-resolution spectra and have derived accurate silicon abundances. Comparing with different Galactic evolution models, e.g. Samland (1998); Goswami & Prantzos (2000); Romano et al. (2010); Kobayashi et al. (2011), these abundances can help astronomers to understand the chemical enrichment history and the origin of the Galaxy. Thus, an accu-

rate measurement of silicon abundances is necessary for many astrophysical applications.

Kamp (1973, 1978, 1982) calculated, both in LTE and NLTE, theoretical equivalent widths and profiles for silicon lines, and compared them with observational data of a dozen early-type stars. The results indicate that the NLTE calculations provided better agreement with observations. The deviations from LTE on Si abundances in the photospheres of the Sun and Vega have been investigated by Wedemeyer (2001), who found that the mean NLTE correction for Si was ~ -0.01 dex for the Sun, and ~ -0.054 dex for Vega. This indicated that the NLTE effects on the Si abundance in the Sun could be neglected, which was confirmed by Shi et al. (2008). Later on, Shi et al. (2009, 2011) systematically investigated the NLTE effects on the derived silicon abundances in the atmospheres of metal-poor stars based on visible lines, and found the NLTE effects are large for the two strong UV lines at 3905 and 4103 Å, especially for warm metal-poor stars. Shi et al. (2012) extended the study to the near-IR *J*-band Si lines, and found that the NLTE effects depend on surface gravities becoming larger for giants. Recently, Bergemann et al. (2013) investigated the NLTE effects on the *J*-band Si lines for red supergiants, and confirmed that Si abundance based on NLTE is significantly lower than that from LTE.

Until very recent, almost all observed high-resolution spectra are from UV, optical, and near-IR *J* bands, therefore, previous studies on NLTE Si abundance are for spectral lines in these three bands. The situation has changed since the Apache Point Observatory Galactic Evolution Experiment (APOGEE) survey² (Majewski et al 2015) (as part of SDSS-

Electronic address: sjr@bao.ac.cn

* Based on observations collected on the 2.16m telescope at Xinglong station, National Astronomical Observatories, Chinese Academy of Sciences, the 2.2m telescope at the Calar Alto Observatory, the 1.88m reflector on the Okayama Astrophysical Observatory, the Kitt Peak coude feed telescope, and the McMath-Pierce solar telescope and the coude focus of the Mayall 4m reflector at Kitt Peak.

² <http://www.sdss.org/surveys/apogee>

III, Eisenstein et al. 2011) started to take high resolution IR H -band spectra for several hundred thousands stars. Thus, it is highly desirable to extend the NLTE investigations to the H -band where there are a dozen Si I lines, which are clearly seen in APOGEE spectra.

Since 2011, the APOGEE survey employs a fiber spectrograph that simultaneously records 300 spectra in the H -band between 1.51 and 1.70 μm at a spectral resolution of $R \sim 22,500$. Detailed information about the instrument was provided by Wilson et al. (2010). Taking advantage of the reduced effect of extinction in IR H -band, APOGEE has observed $\sim 150,000$ stars, predominantly red giants in all major Galactic components accessible from Apache Point Observatory (APO) (Holtzman et al. 2015; Majewski et al 2015). The spectra have been included in the SDSS Data Release 10 (DR10) (Ahn et al. 2014) and SDSS Data Release 12 (DR12) (Alam et al. 2015). The data provide a promising way to trace and explore the formation history of the Galaxy, and they are revolutionizing our knowledge on kinematical and chemical enrichment history of all Galactic stellar populations.

The APOGEE Stellar Parameters and Chemical Abundances Pipeline (ASPCAP) provides the physical and chemical parameters for the APOGEE stars (García Pérez et al. 2016). In addition to the stellar parameters, i.e. the effective temperature (T_{eff}), surface gravity ($\log g$), metallicity ($[\text{M}/\text{H}]$), ASPCAP delivers individual chemical abundances for 15 elements. The accuracy of these derived stellar fundamental parameters and chemical compositions may be compromised. NLTE effects are enhanced by the characteristic low densities, found in the atmospheres of giants, and the absolute reduction in collision rates, thus, affects the atomic populations (Mészáros et al. 2013). Hawkins et al. (2016) have performed an independent procedure to determine the chemical abundances of the APOGEE + Kepler stellar sample (APOKASC) and they inferred that the discrepant phenomenon for some elements is likely due to the NLTE effects. As part of a series of studies on NLTE analysis of H -band lines for several important elements, e.g. Na, Mg, Al, Si, K, Ca, Fe, et al., this work aims to validate the Si atomic model, and to investigate how the abundances derived from the Si H -band transitions are affected by departures from LTE.

This paper is organized as follows. In Section 2, we briefly introduce our adopted Si model atom and NLTE calculation codes, while the selection of the sample stars and the observed spectra are described in Section 3. The stellar parameters of our sample stars are determined in Section 4, and the Si abundances derived from both the H -band and optical lines for the sample stars under LTE and NLTE analysis are presented in Section 5. Finally, the conclusions are given in Section 6.

2. METHOD OF NLTE CALCULATIONS

2.1. Model Atom of Silicon

The Si atomic model that we used here is similar to that of Shi et al. (2008), which includes the most important 132 terms of Si I, 41 terms of Si II, and the Si III ground state. The radiative data are taken from Nahar & Pradhan (1993). Lacking accurate values for incollisions with neutral hydrogen, Shi et al. (2008) suggested $S_{\text{H}} = 0.1$ by fitting solar strong infrared Si I lines. Fortunately, Belyaev et al. (2014) calculated the cross sections and rate coefficients for inelastic processes in Si + H and Si⁺ + H⁺ collisions for all transitions between 26 low-lying states plus the ionic state. We revised the Si atomic model by including all cross sections from

Belyaev et al. (2014) whenever available; Otherwise, $S_{\text{H}} = 0.1$ was adopted. The Grotrian diagram of the silicon model atom with the transitions between 26 low-lying energy terms relative to Belyaev et al. (2014) is shown in Fig. 1. In this work, we also calculated the NLTE line profiles for the Sun and Arcturus with the four different collision treatments, i.e. the Drawin recipe with $S_{\text{H}} = 0.0, 0.1$ and 1.0 and the treatment from Belyaev et al. (2014) and the results are depicted in Fig. 3 and Fig. 4 respectively. Our adopted stellar parameters for the Sun are $T_{\text{eff}} = 5777\text{K}$, $[\text{Fe}/\text{H}] = 0.0\text{dex}$, $\log g = 4.44\text{dex}$ and $\xi_t = 0.9\text{km s}^{-1}$. As shown in these two groups of figures, the calculated NLTE line profiles with $S_{\text{H}} = 0.1$ and the treatment from Belyaev et al. (2014) can fit the observed spectral lines well for both the Sun and Arcturus; for the strong lines at 15888 and 16680 Å, the synthetic line profiles with $S_{\text{H}} = 1.0$ are shallower than the observed ones, while those with $S_{\text{H}} = 0.0$ are slightly deep, with the same silicon abundance.

2.2. Model Atmospheres

We adopted MARCS atmospheric models³, described in detail by Gustafsson et al. (2008). The MARCS models come in two types, the plane-parallel and spherically-symmetric model atmospheres. The models with low surface gravities ($-1.0 \leq \log g \leq 3.5$) are calculated in spherical geometry, while the plane-parallel ones are adopted for stars with $3.0 \leq \log g \leq 5.5$. Gustafsson et al. (2008) suggested that sphericity effects are generally important for the temperature structures of low-gravity stars. In this paper, spherical model atmospheres are used for stars with $\log g \leq 3.5$ and plane-parallel model atmospheres for the others, and they are interpolated with a FORTRAN-based routine coded by Thomas Masseron⁴.

The main characteristics of the MARCS model atmospheres are summarized below (Gustafsson et al. 2008):

- The basic chemical composition of the Sun in model atmospheres is that listed by Grevesse et al. (2007). The adopted solar Si abundance is 7.51 dex, which is the 3D-based LTE Si abundance and also the meteoritic Si abundance. Amarsi & Asplund (2016) recently based on a 3D NLTE calculations also found the same solar Si abundance.
 - The α -enhancement is included.
- $$[\alpha/\text{Fe}] = \begin{cases} 0.4 \cdot |[\text{Fe}/\text{H}]| & \text{if } -1.0 < [\text{Fe}/\text{H}] < 0.0 \\ 0.4 & \text{if } [\text{Fe}/\text{H}] \leq -1.0 \end{cases}$$
- The adopted mixing-length parameter l/H_p is 1.5 (Heney et al. 1965).

2.3. Statistical Equilibrium Codes

A revised version of DETAIL program (Butler & Giddings 1985) was adopted to solve the coupled statistical equilibrium and the radiative transfer equations. This program is based on an accelerated lambda iteration scheme, following the approach described by Rybicki & Hummer (1991, 1992). In this paper, departure coefficients were computed with DETAIL, and then fed to the spectrum synthesis software package Spectrum Investigation Utility (SIU), developed by Reetz (1991) to derive chemical abundances.

³ <http://marcs.astro.uu.se>

⁴ <http://marcs.astro.uu.se/software.php>

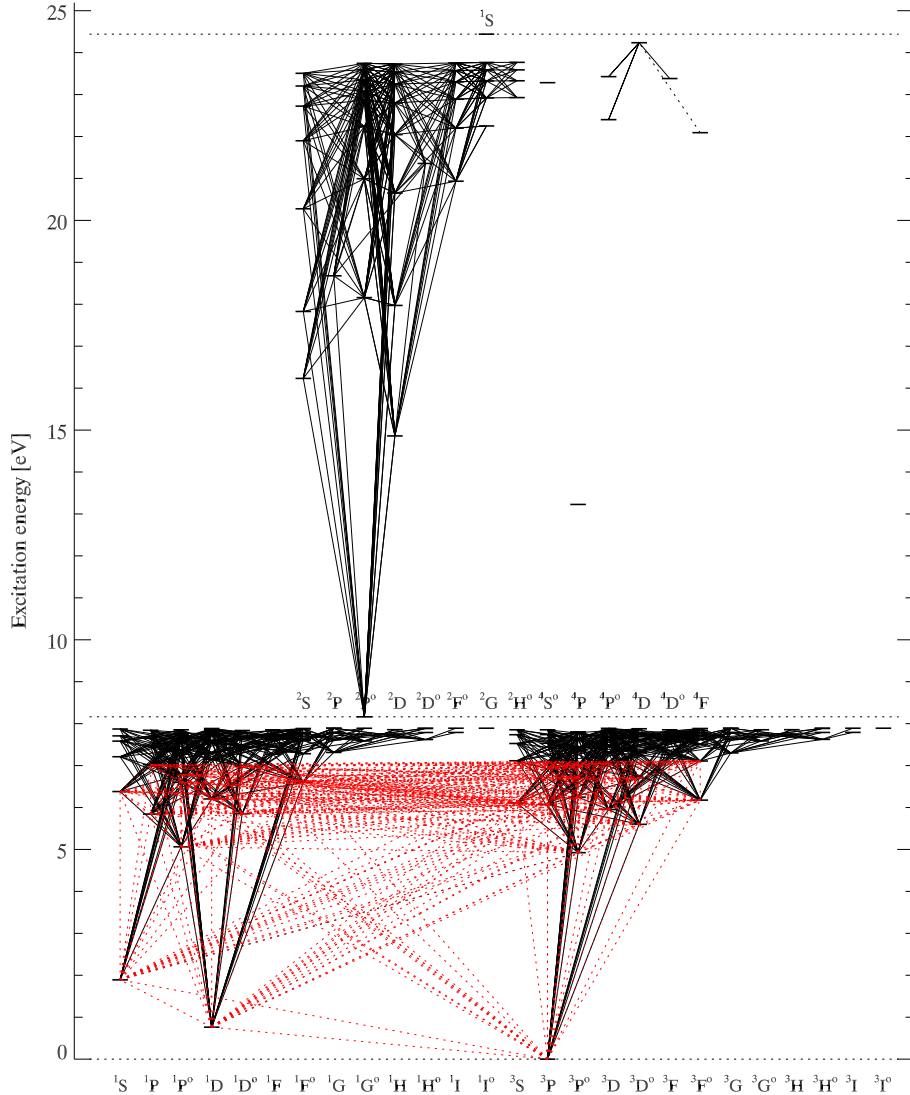


FIG. 1.— Grotrian diagram of the silicon model atom. Si II quartets are neglected. Allowed transitions are black continuous, the forbidden Si I 4103Å line is black dotted. Transitions of Si I between 26 low-lying energy terms presented by Belyaev et al. (2014) are shown with red-dotted lines.

3. THE SAMPLE STARS AND THEIR SPECTRA

3.1. Sample Selection

Although Shi et al. (2012) have demonstrated that their Si atomic model could provide consistent silicon abundances for the optical and infrared J -band spectra, we would like to check whether the atomic model can also be applied to the H -band Si I lines. We selected 13 FGK dwarfs and giants as sample stars for this test according to the following criteria: 1) they must have available high-resolution ($R > 20,000$) and high signal-to-noise ratio ($S/N > 100$) spectra both in the optical and H band; 2) the selected stars should be representative of the typical stellar parameter range of the FGK stars ($T_{\text{eff}} \sim 4000 - 6500$ K, $\log g \sim 0.0 - 5.0$, and $[M/H] \sim -2.0 - 0.5$ dex). The final stellar parameters of sample stars span from 4275 to 6070 K for T_{eff} , from 1.67 to 4.65 for $\log g$, and from -1.35 to 0.28 dex for $[Fe/H]$. However, there are no very metal-poor stars ($[Fe/H] < -1.5$ dex) in our sample, due to the

weakness of Si lines in the APOGEE spectra for such stars. The IR and optical data are described in the following subsections.

3.2. Infrared H -band Spectra

The IR H -band spectra of our 13 sample stars are from the NMSU 1m+APOGEE observations, and they are included in SDSS DR12. The 1m+APOGEE configuration is designed to observe nearby bright stars and to provide an improved calibration for the main APOGEE survey (Holtzman et al. 2015). A bundle of ten fibers was installed connecting the APOGEE instrument to the NMSU (New Mexico State University) 1m telescope. This configuration provides one science fiber and nine sky fibers per observation. Bright stars with magnitude of $0 < H < 8$ are observed in this configuration in dark time when the APOGEE instrument is not connected with the Sloan 2.5m Telescope. The spectra taken with the NMSU 1m+APOGEE are reduced and analyzed with the same soft-

were employed by the main survey (Nidever et al. 2015). We refer the reader to Feuillet et al. (2016) for more details. Since all 13 selected stars are bright, the S/N of APOGEE spectra of these stars are very high (e.g. $S/N \geq 400$ for Arcturus). As mentioned earlier, the resolution is about 22,500.

The high-resolution ($R \sim 500,000$) solar infrared spectrum from Kurucz website⁵ was adopted in this study. It was obtained by James Brault at Kitt Peak and reduced by Robert L. Kurucz. We also employed the spectrum of Arcturus from the NOAO science archives⁶, which was recorded with the Fourier transform spectrometer (FTS, Hall et al. 1979) operated at the coudé focus of the Mayall 4m reflector at Kitt Peak. The detailed description of the observation was presented by Hinkle et al. (1995). The high-resolution ($\sim 100,000$) and high signal-to-noise ratio spectrum of Arcturus makes it easier to identify the continuum, and most efficient to recognize blending lines.

3.3. Optical Spectra

We adopted the optical solar spectrum of Kurucz et al. (1984). Six of our sample stars (HD 6582, HD 6920, HD 102870, HD 103095, HD 121370, HD 148816) were observed with the fiber-coupled Cassegrain échelle spectrograph (FOCES; Pfeiffer et al. 1998) on the 2.2m telescope at the Calar Alto Observatory. Spectra of HD 87, HD 22675, HD 58367, and HD 177249 were taken with the High Dispersion Échelle Spectrograph (HIDES) on the coudé focus of the 1.88m reflector at the Okayama Astrophysical Observatory (Izumiura 2003). The optical spectrum of Arcturus was obtained with the échelle spectrograph (ES) on the Kitt Peak coudé feed telescope (KPCFT), with a typical resolving power of 150,000, and a S/N of about 1,000 (Hinkle et al. 2000, 2005). Both HD 31501 and HD 67447 were observed using the 2.16m telescope at Xinglong station but with different spectrographs, for HD 31501 with the Coudé Échelle Spectrograph (CES; Zhao & Li 2001) and for HD 67447 with the fiber optics échelle spectrograph (FOES). The detailed observational information for the sample stars is listed in Table 1 (except the Sun). It is worthwhile noting that all optical spectra have a resolving power better than 35,000 and $S/N \geq 150$.

4. STELLAR PARAMETERS

The stellar parameters of all 13 stars were determined via the spectroscopic approach. Specifically, the effective temperature and surface gravity were determined by fulfilling the excitation equilibrium of Fe I and the ionization equilibrium of Fe I and Fe II, respectively; the micro-turbulence velocity was determined by forcing $[Fe/H]$ from different Fe I lines to be independent of their equivalent widths. Table 8 gives the equivalent widths for our sample stars.

This process of determining stellar parameters is an iterative procedure. A set of initial parameters is needed to begin with. The initial temperature was derived from the Balmer lines (H_α and H_β) (Fuhrmann 1998) if these lines were available. Otherwise, it was obtained based on the color index ($b - y$ or $V - K$) employing the calibration given by Alonso et al. (1996, 1999, 2001); The initial surface gravity was estimated using the parallax method. There are 30 Fe I and six Fe II optical lines included in our analysis. The line data as well as the equivalent widths for the solar iron lines are

listed in Table 6. Departures from LTE have been considered when determining the iron abundance based on the iron model atom from Mashonkina et al. (2011) and for the Sun and our sample stars, they are small, less than 0.05 dex. In Table 6, we also present the solar LTE and NLTE iron abundances based on the oscillator strengths ($\log gf$) values recommended by the VALD3 database⁷. According to this table, the iron abundances derived from Fe I lines are 7.56 ± 0.13 dex in LTE and 7.60 ± 0.13 dex in NLTE, while they are 7.49 ± 0.04 dex from Fe II lines in both cases. The statistical error for the Sun is uncomfortably large, up to 0.13 dex, thus we derived the empirical $\log gf$ by fitting the solar spectrum and presented the NLTE one in this table. The values of $\log C_6$ were calculated referring to Anstee & O'Mara (1991, 1995) and Barklem et al. (2000). Based on multiple iterative processes, we estimated the typical uncertainties of T_{eff} , $\log g$, $[Fe/H]$, and ξ_t are ± 80 K, ± 0.1 dex, ± 0.08 dex, and 0.2 km s^{-1} respectively.

The final derived stellar parameters, along with stellar parameters for the same stars from the literature, are presented in Table 2. Our derived values are consistent with those from literature, except $\log g$ for HD 22675 and HD 177249. Our newly derived $\log g$ values for the two stars are 0.26 and 0.11, respectively, higher than those determined by Takeda et al. (2008). We note that our spectroscopic $\log g$ values agree well with those from the parallax method derived by Takeda et al. (2008). This may indicate that our spectroscopic surface gravities for these two stars are better than those from Takeda et al. (2008).

5. NLTE CALCULATIONS FOR SAMPLE STARS

5.1. Line Data

5.1.1. Infrared Atomic Line Data in the H band

Initially, we found 11 Si I lines in the H -band APOGEE spectra. A further investigation reveals that seven of them are very weak or heavily blended. As a result, only four lines were employed in this study. The details about them are presented in Table 3. The transitions are taken from the NIST database⁸. The van der Waals damping constants ($\log C_6$) are extracted from Meléndez et al. (1999), who calculated C_6 based on the quantum-mechanical approximate cross sections provided by Anstee & O'Mara (1995), Barklem & O'Mara (1997) and Barklem et al. (1998). We derived the solar LTE and NLTE Si abundances using the gf -values referring to the references and found that the statistic errors are very large in both LTE and NLTE. In order to reduced the importance of oscillator strengths, therefore, we performed a line-to-line differential analysis and the gf -values derived from the LTE and NLTE solar spectrum fits are also listed in Table 3.

5.1.2. Optical Atomic Line Data

We started with the same set of neutral Si optical lines used by Shi et al. (2009). An examination shows that the line at 3905 \AA is severely blended with a CH line, and the line at 4103 \AA falls in the wing of H_δ , while the line at 5690 \AA is blended with an iron line. These three transitions were excluded from our Si abundance analysis. The adopted eight Si I lines and line data are listed in Table 3. We also derived the solar Si abundance based on optical lines using the $\log gf$

⁵ <http://kurucz.harvard.edu/sun/irradiance2008/>

⁶ <http://ast.noao.edu/data/other>

⁷ <http://vald.astro.uu.se>

⁸ <http://physics.nist.gov/>

TABLE 1
CHARACTERISTICS OF THE OBSERVED OPTICAL SPECTRA

Star	V_{mag}^1 (mag)	Telescope/spectrograph	Observing run, observer	Spectral range (Å)	R	S/N
Arcturus	−0.05	KPCFT/ES	1998-99, Hinkle K. et al.	3727-9300	150,000	~ 1,000
HD 87	5.55	1.88-m/HIDES	Jul. 2007, Anonymous ²	5000-6200	67,000	≥ 150
HD 6582	5.17	2.2-m/FOCES	Sep. 1995, Fuhrmann K.	4000-7000	35,000	≥ 150
HD 6920	5.67	2.2-m/FOCES	Feb. 1997, Fuhrmann K.	4000-9000	60,000	~ 200
HD 22675	5.86	1.88-m/HIDES	Jan. 2010, Sato B.	4000-7540	67,000	~ 300
HD 31501	8.15	2.16-m/CES	Jan. 2008, Shi J.R.	5600-8800	40,000	≥ 150
HD 58367	4.99	1.88-m/HIDES	Feb. 2004, Anonymous ²	5000-6200	67,000	≥ 150
HD 67447	5.34	2.16-m/FOES	Jan. 2015, Zhang J.B.	3900-7260	50,000	≥ 150
HD 102870	3.59	2.2-m/FOCES	May. 1997, Fuhrmann K.	4000-9000	60,000	~ 200
HD 103095	6.42	2.2-m/FOCES	May. 2000, Fuhrmann K.	4000-9000	60,000	~ 200
HD 121370	2.68	2.2-m/FOCES	Dec. 1998, Fuhrmann K.	4000-9000	60,000	~ 200
HD 148816	7.27	2.2-m/FOCES	Aug. 2001, Gehren T.	4000-9000	60,000	~ 200
HD 177249	5.51	1.88-m/HIDES	Nov. 2004, Anonymous ²	5000-6200	67,000	~ 300

¹ Visual magnitudes are derived from the Hipparcos Main Catalogue (ESA 1997) through VizieR^a.

² Spectra were provided by Takeda Y., Sato, B. and Liu Y.J. et al. The observer written in the spectra header is anonymous, and it is difficult for us to identify the actual observers.

^ahttp://vizier.u-strasbg.fr/viz-bin/VizieR.

TABLE 2
COMPARISON OF STELLAR PARAMETERS WITH OTHER STUDIES

Star	T_{eff} (K)	$\log g$ [cgs]	[Fe/H]	ξ_t km s ^{−1}	Ref. ^a
Arcturus	4275	1.67	−0.58	1.60	This study
	4286	1.66	−0.52	1.74	RAM11
	4286	1.66	−0.48	1.74	SHE15
HD 87	5053	2.71	−0.10	1.35	This study
	5072	2.63	−0.10	1.35	TAK08
HD 6582	5390	4.42	−0.81	0.90	This study
	5387	4.45	−0.83	0.89	FUH98
HD 6920	5845	3.45	−0.06	1.40	This study
	5838	3.48	−0.05	1.35	FUH98
HD 22675	4901	2.76	−0.05	1.30	This study
	4878	2.50 ^b	−0.06	1.29	TAK08
		2.66 ^c			TAK08
HD 31501	5320	4.45	−0.40	1.00	This study
	5326	4.41	−0.38	1.00	WAN09
HD 58367	4932	1.79	−0.18	2.00	This study
	4911	1.76	−0.14	2.04	TAK08
HD 67447	4933	2.17	−0.05	2.12	This study
	4974	2.12	−0.06	2.12	TAK08
HD 102870	6070	4.08	0.20	1.20	This study
	6085	4.04	0.14	1.38	FUH98
	6060	4.11	0.18	1.20	MAS11
HD 103095	5085	4.65	−1.35	0.80	This study
	5110	4.66	−1.35	0.85	FUH98
	5070	4.69	−1.35	0.80	MAS07
HD 121370	6020	3.80	0.28	1.40	This study
	6023	3.76	0.28	1.40	FUH98
HD 148816	5830	4.10	−0.73	1.40	This study
	5823	4.13	−0.73	1.40	NIS10
HD 177249	5273	2.66	0.03	1.65	This study
	5251	2.55 ^b	0.00	1.65	TAK08
		2.62 ^c			TAK08

NOTE. — Underlines mean these stars with them are discussed in detail in Section 4.

^a RAM11: Ramírez & Allende Prieto (2011), SHE15: Sheminova (2015), TAK08: Takeda et al. (2008), FUH98: Fuhrmann (1998), WAN09: Wang et al. (2009), MAS11: Mashonkina et al. (2011), MAS07: Mashonkina et al. (2007), NIS10: Nissen & Schuster (2010)

^b $\log g$ derived from the spectroscopic method

^c $\log g$ derived from the parallax and evolution-track method

values from references. Although the mean Si abundance is consistent with the previous studies, the statistic error is also not satisfying, up to 0.1 dex. To be consistent with the situ-

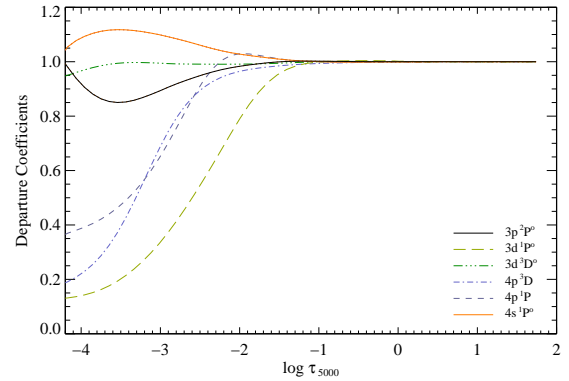


FIG. 2.— Departure coefficients $b_i = N_i^{\text{NLTE}}/N_i^{\text{LTE}}$ as a function of the standard optical depth for HD 87.

ation for infrared lines, we also present the gf -values determined from the solar spectrum fitting. The C_6 values were calculated according to Anstee & O'Mara (1991, 1995) and Barklem et al. (2000).

5.2. NLTE Effects

5.2.1. Departures from LTE for the Si I H -band lines

In Fig. 2, we present the departure coefficients (b_i) for the relevant Si I levels for H -band transitions and Si II ground state as a function of the optical depth at $\lambda = 5000$ Å (τ_{5000}) for the model atmosphere of HD 87. Here, the departure coefficients (b_i) are defined as $b_i = n_i^{\text{NLTE}}/n_i^{\text{LTE}}$, where n_i^{NLTE} and n_i^{LTE} represent the statistical equilibrium (NLTE) and thermal (LTE) atomic level number densities, respectively. It is found that the departure coefficients for the level $3d^3D^o$ of Si I are near their thermal value ($b_i \sim 1$) and the level $4s^1P^o$ are overpopulated, while the other excitation levels, $4p^1P$, $4p^3D$, $3d^1P^o$, are underpopulated due to photon loss (see Fig. 2 for details).

As the first test of our atomic model, we have analyzed optical lines for the Sun. We confirmed that the NLTE corrections for optical silicon lines are negligible (Shi et al. 2008; Wedemeyer 2001; Bergemann et al. 2013). For the investigated four H -band Si lines, we found that the derived NLTE

TABLE 3
ATOMIC DATA OF THE SILICON OPTICAL AND H -BAND LINES, THE DERIVED LTE AND NLTE SOLAR SILICON ABUNDANCE
BASED ON $\log gf$ FROM REFERENCES AND THE NLTE CORRECTIONS FOR THE SOLAR SILICON LINES

λ (Å)	Transition	χ (eV)	$\log C_6$	$\log gf$	Ref.	$\log \epsilon_{\odot}$ Si LTE (dex)	$\log \epsilon_{\odot}$ Si NLTE (dex)	$\log gf'$ LTE	$\log gf'$ NLTE	Δ_{\odot} (dex)
5701.104	$4s^3P_1^o - 5p^3P_0$	4.930	-30.094	-2.05	GAR73,KEL08	7.60	7.60	-1.96	-1.96	0.00
5772.146	$4s^1P_1^o - 5p^1S_0$	5.082	-30.087	-1.75	GAR73,KEL08	7.64	7.63	-1.62	-1.63	-0.01
6142.483	$3p^3D_1^o - 5f^3D_3$	5.619	-29.669	-1.30	KUR07	7.37	7.37	-1.44	-1.44	0.00
6145.016	$3p^3D_2^o - 5f^3G_3$	5.616	-29.669	-1.31	KUR07	7.45	7.45	-1.37	-1.37	0.00
6155.134	$3p^3D_3^o - 5f^3G_4$	5.619	-29.669	-0.76	KUR07	7.50	7.49	-0.77	-0.78	-0.01
6237.319	$3p^3D_0^o - 5f^3F_2$	5.614	-29.669	-0.98	KUR07	7.43	7.43	-1.06	-1.06	0.00
6243.815	$3p^3D_2^o - 5f^3F_3$	5.616	-29.669	-1.24	KUR07	7.49	7.49	-1.26	-1.26	0.00
6244.466	$3p^3D_2^o - 5f^1D_2$	5.616	-29.669	-1.09	KUR07	7.35	7.35	-1.25	-1.25	0.00
mean						7.48	7.48			
σ						0.10	0.10			
15888.440	$4s^1P_1^o - 4p^1P_1$	5.082	-30.638	0.06	KUR07	7.58	7.57	0.13	0.12	-0.01
16380.177	$4p^1P_1 - 3d^1P_1^o$	5.863	-30.495	-0.47	KUR07	7.03	7.03	-0.95	-0.95	0.00
16680.810	$4p^3D_3 - 3d^3D_3^o$	5.984	-30.357	-0.14	KUR07	7.48	7.45	-0.17	-0.20	-0.03
16828.158	$4p^3D_3 - 3d^3D_2^o$	5.984	-30.357	-1.03	KUR07	7.41	7.41	-1.13	-1.13	0.00
mean						7.37	7.36			
σ						0.24	0.24			

NOTE. — References to the $\log gf$ values are GAR73 : Garz (1973), KEL08 : Kelleher & Podobedova (2008) and KUR07 : Kurucz (2007). The $\log C_6$ values were calculated according to Anstee & O'Mara (1991, 1995) and Barklem et al. (2000). σ refers to the statistical error. The $\log gf'$ denotes that the gf -values were derived from the solar fits.

effects are also minor and the largest one is 0.03 dex (see Table 3). A comparison between the calculated H -band line profiles and the observed solar spectrum is shown in Fig. 3. In this figure, the NLTE (black solid) lines agree well with the observed spectrum for the strong lines at 15888 and 16680 Å, while the LTE (red dotted) line profiles are weaker. This issue is more obvious for Arcturus, as presented in Fig. 4. Fig. 5 gives the synthetic profiles at 16680 Å under LTE and NLTE for HD 87. The black solid line denotes the best fit to the observed spectrum in NLTE with a $[\text{Si}/\text{Fe}]$ of 0.12 dex. The red dotted curve is produced with the same $[\text{Si}/\text{Fe}]$ in LTE, which is shallower in the line core.

In Table 4, we present the Si abundances derived from the individual H -band lines and the mean line-to-line scatter under NLTE and LTE for all sample stars. As indicated in this table, relative to LTE, NLTE obviously reduces the line-to-line scatter in the derived abundances for some stars. Taking HD 67447 as an example, the mean line-to-line scatter is reduced from 0.12 in LTE to 0.03 dex in NLTE. Table 5 gives the mean abundances along with the standard deviation. As shown in this table, the largest standard deviation in LTE is 0.12 dex, however, it decreases to 0.07 dex, when the NLTE effects are considered.

According to Table 4, the NLTE effects differ from line to line, and they are larger for strong lines. Among our four H -band lines, NLTE effects are relatively strong for the Si I lines at 15888 and 16680 Å while they are smaller for the others. Table 5 also shows the mean NLTE corrections for individual stars and the NLTE effects are from -0.1 to 0.0 dex.

To explore the dependency of the NLTE corrections on stellar parameters, we plotted the difference of the $[\text{Si}/\text{Fe}]$ derived under NLTE and LTE assumptions for the strong silicon lines (15888 and 16680 Å) as functions of metallicity, effective temperature, and surface gravity in Fig. 6. It can be seen that the NLTE corrections of the H -band lines are negative, which means that the Si abundances would be overestimated under LTE; and that the NLTE effects are very sensitive to the surface gravity, the absolute corrections increase with the de-

creasing surface gravity, and the largest one reaches ~ 0.2 dex for HD 58367. Since surface gravity effects dominate, we do not see clear trends in the NLTE corrections with metallicity and effective temperature in these figures. In order to investigate the NLTE corrections for APOGEE data in extreme cases, we calculated the NLTE and LTE line profiles of the Si I line at 15888 Å with parameters $T_{\text{eff}} = 5000$ K, $[\text{Fe}/\text{H}] = 0.0$ dex, $\log g = 0.5$, $\xi_r = 2.0$ km s $^{-1}$. As shown in Fig. 7, when $[\text{Si}/\text{Fe}]$ under NLTE and LTE shares the same value, namely $[\text{Si}/\text{Fe}] = 0.0$ dex, the two profiles are different. By increasing $[\text{Si}/\text{Fe}]$, the line cores of LTE spectra tend to be deeper and, until $[\text{Si}/\text{Fe}]$ reaches 0.39 dex, the LTE profile best fits the synthetic NLTE one. That is to say that in this extreme case, the NLTE correction can reach ~ -0.4 dex.

To test whether consistent abundances are obtained from spectra acquired with different telescopes/instruments, we derived the Si abundance of Arcturus with the spectrum from Hinkle et al. (1995) ($R \sim 100,000$) and the 1m+ APOGEE spectrum ($R \sim 22,500$). Fig. 8 demonstrates the best NLTE fitting profiles for the two observed spectra. The left panel is for the Arcturus spectrum from Hinkle et al. (1995) while the right one is for the 1m+APOGEE. Their results for individual lines are listed in Table 4 and the mean ones in Table 5. The difference of abundances derived from individual lines between the two spectra is negligible, ≤ 0.02 dex. A consistent Si abundance is acquired for the same object from different telescopes/instruments.

5.2.2. Departures from LTE for Si I optical lines

We investigated the eight Si I optical lines described in Subsection 5.1.2 for our sample stars. The mean Si abundances under LTE and NLTE are presented in Table 5. As shown in this table, the standard deviations are very small, less than 0.05 dex for both LTE and NLTE abundances; the net NLTE correction for a given star is minor, with an absolute value less than 0.06 dex. Although the mean NLTE corrections are small, the NLTE effects are necessary for the strongest investigated Si I lines, e.g. the largest NLTE correction for the line

TABLE 4
STELLAR [Si/Fe] FOR THE INDIVIDUAL Si I H-BAND LINES UNDER LTE AND NLTE ANALYSES

Star	15888 (Å)		16380 (Å)		16680 (Å)		16828 (Å)		σ_{line}	
	LTE	NLTE	LTE	NLTE	LTE	NLTE	LTE	NLTE	LTE	NLTE
Arcturus ^a	0.49	0.38	0.37	0.36	0.43	0.32	0.43	0.42	0.06	0.05
Arcturus ^b	0.50	0.38	0.34	0.33	0.44	0.34	0.44	0.43	0.08	0.06
HD 87	0.19	0.08	0.15	0.14	0.23	0.12	0.15	0.15	0.05	0.04
HD 6582	0.22	0.19	0.26	0.25	0.26	0.25			0.03	0.04
HD 6920	0.11	-0.01	-0.04	-0.05	0.10	-0.01			0.10	0.03
HD 22675	0.12	0.02	0.07	0.06	0.15	0.06			0.05	0.03
HD 31501	0.13	0.09	0.16	0.15	0.21	0.19			0.05	0.07
HD 58367	0.26	0.03	0.04	0.04	0.31	0.13	0.12	0.13	0.16	0.07
HD 67447	0.25	0.08	0.05	0.04	0.22	0.07	0.10	0.10	0.12	0.03
HD 102870	-0.02	-0.09	-0.07	-0.08	-0.04	-0.09	-0.08	-0.08	0.04	0.01
HD 103095	0.26	0.24	0.36	0.36	0.35	0.35			0.07	0.08
HD 121370	0.11	0.02	0.15	0.14	0.22	0.14	0.14	0.14	0.06	0.06
HD 148816	0.30	0.24	0.21	0.20	0.27	0.23			0.06	0.03
HD 177249	0.20	0.07			0.20	0.06	0.08	0.08	0.08	0.01

NOTE. — σ_{line} denotes the mean line-to-line scatter.

^a The H-band spectrum of Arcturus is from Hinkle et al. (1995).

^b The H-band spectrum of Arcturus is the NMSU 1m + APOGEE one.

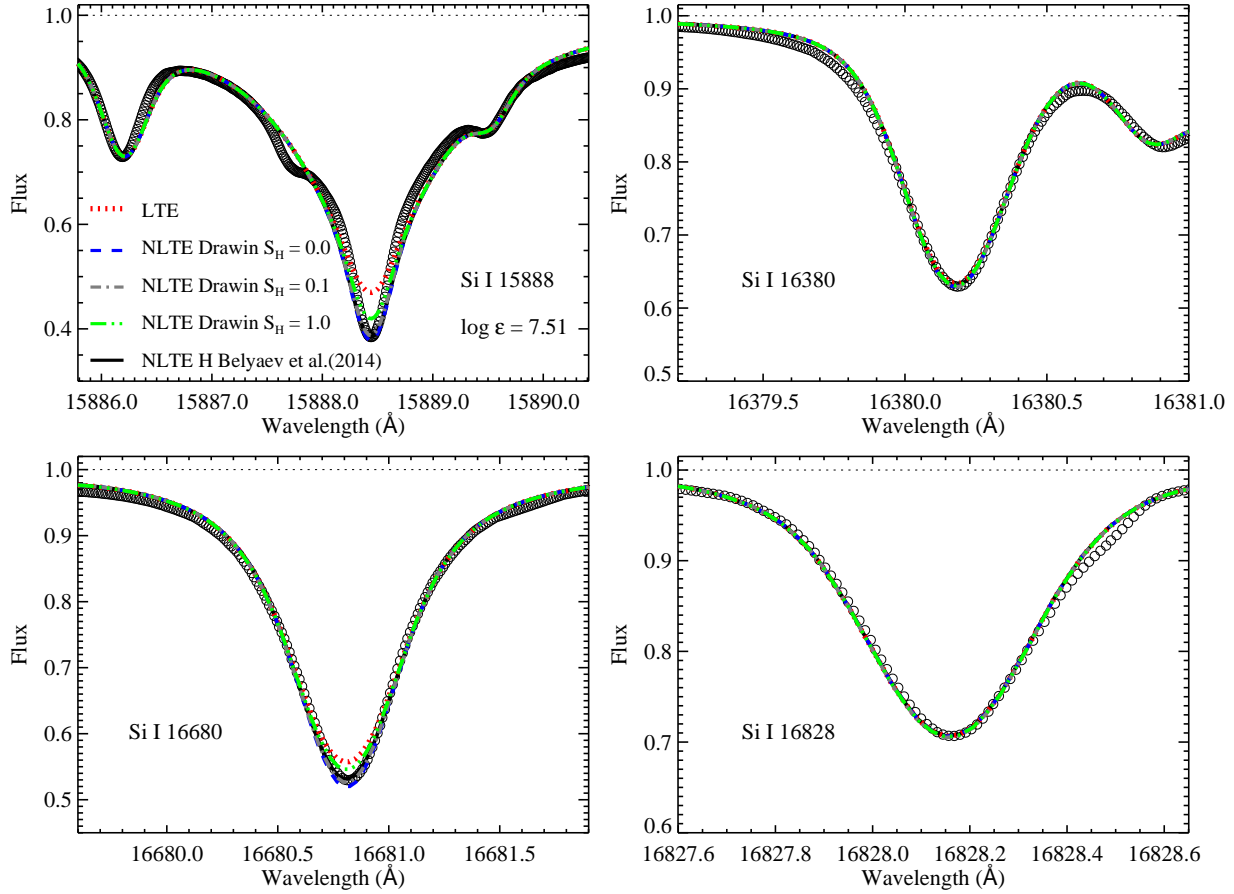


FIG. 3.— *H*-band solar Si I line profiles. The NLTE profiles with rates of collisions with hydrogen from Belyaev et al. (2014) and the Drawin recipe with $S_H = 0.0, 0.1, 1.0$, and LTE ones compared with the observed spectrum (open circles), where the NLTE profiles with the Belyaev et al. (2014) treatment refer to the best fits.

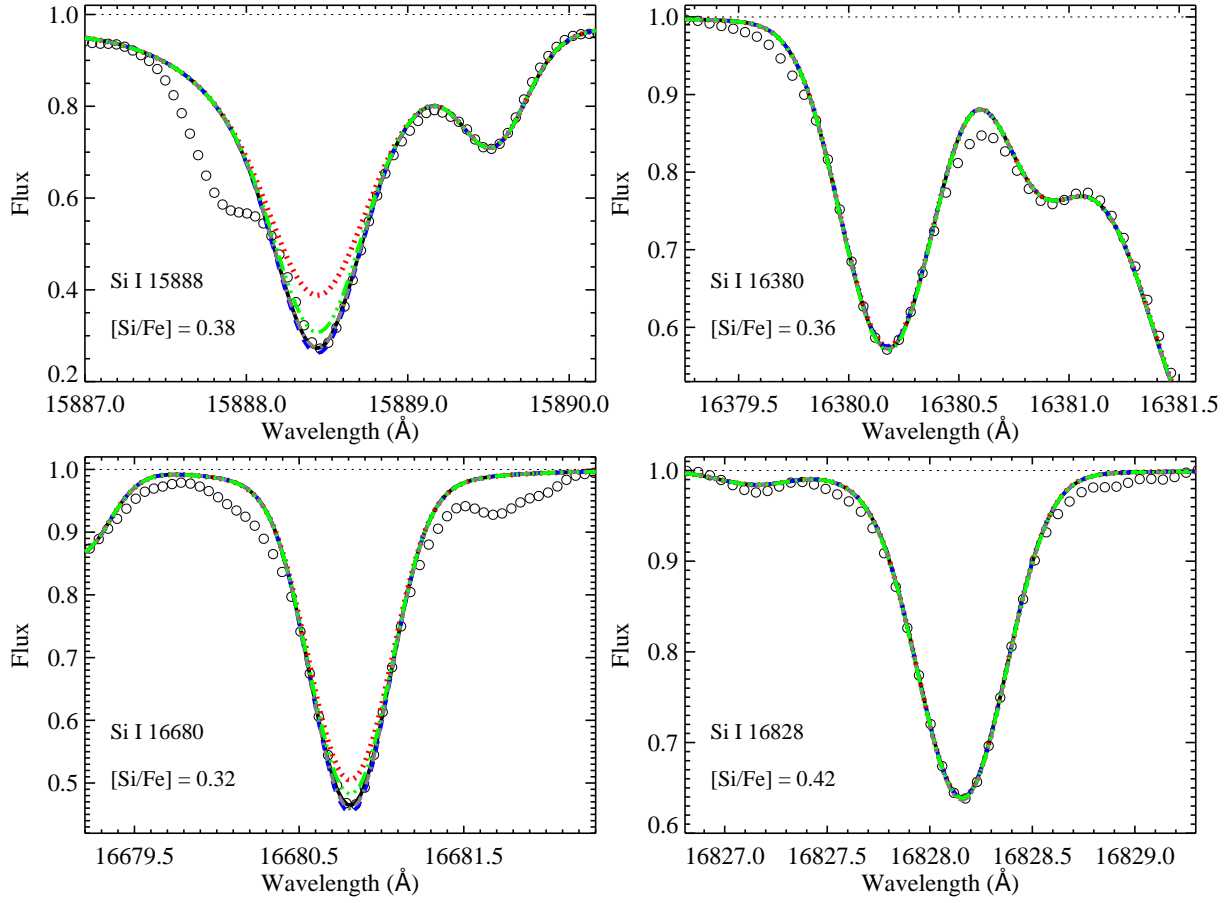


FIG. 4.— Similar to Fig. 3, the NLTE and LTE profiles for Arcturus. Here the observed spectrum is from Hinkle et al. (1995).

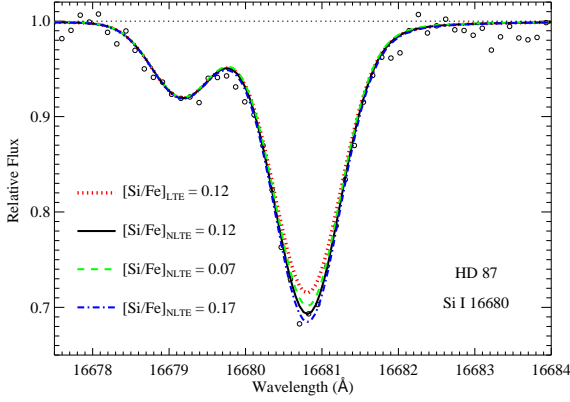


FIG. 5.— Spectrum synthesis of the Si I 16680 Å line for HD87. The open circles are the observed spectrum; the black solid line is the best-fitting NLTE line profile and the red dotted curve is the LTE profile with the same Si abundance; the other two lines are the synthetic spectra in NLTE with different $[\text{Si}/\text{Fe}]$ (see the legend for details).

at 6155 Å reaches ~ 0.1 dex in our sample according to Table 7. The corrections could be greater in extreme cases.

5.2.3. Comparison with the Optical Results and Discussions

For our sample stars, the differences between the mean Si abundances derived from IR and from optical spectra are shown against the metallicity in Fig. 9. In this figure, open circles denote the differences in LTE while filled circles indicate the NLTE results. As one can see, the differences between LTE and NLTE are small (less than 0.1 dex) and the derived Si abundances from the H -band spectral lines agree better with those from optical lines in NLTE than in LTE. Since the NLTE effects are larger for strong lines, it is interesting to see whether the Si abundances derived when only H -band strong lines at 15888 and 16680 Å available are still consistent with the ones from optical lines. The differences between the abundances derived from the two strong H -band lines and from optical lines are depicted in Fig. 10. Similar to Fig. 9, the NLTE Si abundances from the strong H -band lines are consistent with those from optical lines, while the differences become as large as 0.2 dex in LTE.

6. CONCLUSIONS

The main purpose of this work is to test the validity of the Si atomic model for H -band line formation, and to investigate the NLTE effects on Si spectral lines based on high S/N IR H -band spectra. A sample of 13 FGK dwarfs and giants was selected, and the Si abundances were derived from both H -band and optical lines under LTE and NLTE.

After careful analysis, we conclude that:

- With a NLTE analysis, the absolute differences between the mean Si abundances from the H -band and from optical lines are less than 0.1 dex for the sample stars, which suggests that our Si atomic model can be applied for investigating the formation of the H -band Si I lines.
- The NLTE effects differ from line to line. The strong Si I lines at 15888 and 16680 Å need large NLTE corrections, while the other two lines show weaker NLTE effects. Thus, it is not surprising that the NLTE silicon abundance shows a smaller line-to-line scatter than the LTE one for some stars in this analysis. The NLTE

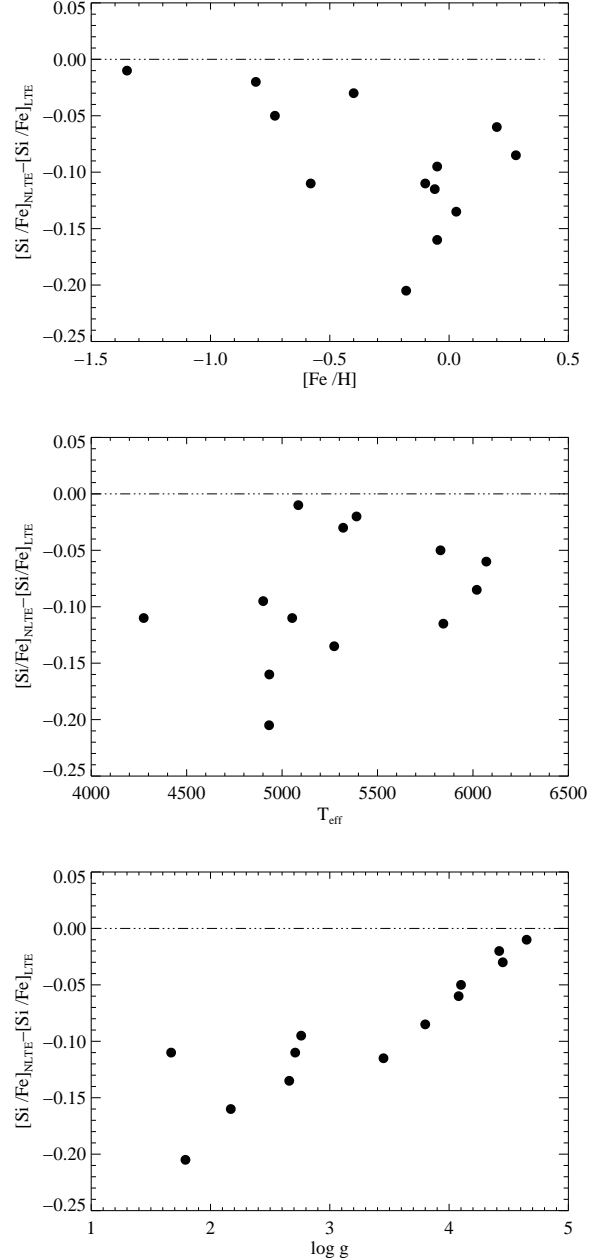


FIG. 6.— The mean NLTE corrections for the two strong Si I lines at 15888 and 16680 Å as functions of $[\text{Fe}/\text{H}]$, T_{eff} , and $\log g$ respectively (from top to bottom).

corrections reach ~ -0.2 dex for the strongest Si I line among our sample. It can be up to ~ -0.4 dex for the extreme cases of APOGEE targets ($\log g \sim 0.5$). Thus it should be considered in the abundance analysis, especially for the cases where only strong lines are available.

- The NLTE effects are sensitive to the surface gravity, and increase with decreasing surface gravity.
- The NLTE corrections for the investigated H -band lines are negative, which means that the Si abundances derived with LTE assumption will be overestimated.

To the best of our knowledge, this work is the first NLTE

TABLE 5
STELLAR SILICON LTE AND NLTE ABUNDANCES

Star	T_{eff}	$\log g$	[Fe/H]	ξ_i	[Si I _{LTE} /Fe](ir)	[Si I _{NLTE} /Fe](ir)	Δ_{ir}	[Si I _{LTE} /Fe](opt)	[Si I _{NLTE} /Fe](opt)	Δ_{opt}
Arcturus ^a	4275	1.67	-0.58	1.60	0.43±0.05	0.37±0.04	-0.06	0.35±0.03	0.29±0.02	-0.06
Arcturus ^b	4275	1.67	-0.58	1.60	0.43±0.07	0.37±0.05	-0.06			
HD 87	5053	2.71	-0.10	1.35	0.18±0.04	0.12±0.03	-0.06	0.15±0.03	0.12±0.01	-0.03
HD 6582	5390	4.42	-0.81	0.90	0.25±0.02	0.23±0.03	-0.02	0.27±0.02	0.27±0.02	0.00
HD 6920	5845	3.45	-0.06	1.40	0.06±0.08	-0.02±0.02	-0.08	0.05±0.05	0.02±0.03	-0.03
HD 22675	4901	2.76	-0.05	1.30	0.11±0.04	0.05±0.02	-0.06	0.11±0.04	0.07±0.02	-0.04
HD 31501	5320	4.45	-0.40	1.00	0.17±0.04	0.14±0.05	-0.03	0.22±0.02	0.21±0.02	-0.01
HD 58367	4932	1.79	-0.18	2.00	0.18±0.12	0.08±0.06	-0.10	0.16±0.05	0.13±0.02	-0.03
HD 67447	4933	2.17	-0.05	2.12	0.16±0.10	0.07±0.02	-0.09	0.12±0.04	0.08±0.02	-0.04
HD 102870	6070	4.08	0.20	1.20	-0.05±0.03	-0.09±0.01	-0.04	-0.07±0.02	-0.08±0.02	-0.01
HD 103095	5085	4.65	-1.35	0.80	0.32±0.06	0.32±0.07	0.00	0.30±0.04	0.30±0.04	0.00
HD 121370	6020	3.80	0.28	1.40	0.16±0.05	0.11±0.06	-0.05	0.22±0.05	0.19±0.03	-0.03
HD 148816	5830	4.10	-0.73	1.40	0.26±0.05	0.22±0.02	-0.04	0.18±0.03	0.18±0.03	0.00
HD 177249	5273	2.66	0.03	1.65	0.16±0.07	0.07±0.01	-0.09	0.05±0.04	0.03±0.02	-0.02

NOTE. — Δ_{ir} and Δ_{opt} stand for the NLTE effects ($\Delta = \log \epsilon_{\text{NLTE}} - \log \epsilon_{\text{LTE}}$) derived from IR and optical spectra respectively.

^a The *H*-band spectrum of Arcturus is from Hinkle et al. (1995).

^b The *H*-band spectrum of Arcturus is the NMSU 1m + APOGEE one.

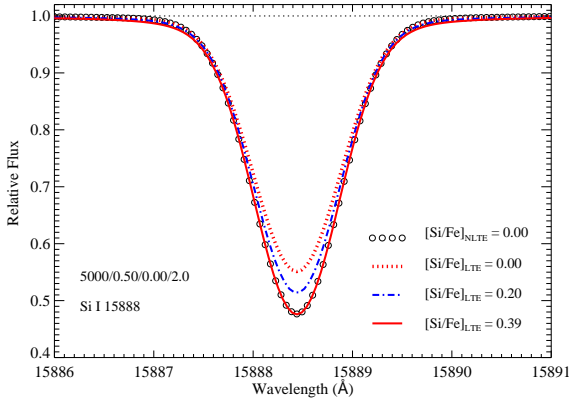


FIG. 7.— The LTE and NLTE synthetic spectra of Si I 15888 Å line with different [Si/Fe] values and the same parameters of $T_{\text{eff}} = 5000$ K, $\log g = 0.5$, [Fe/H] = 0.0, $\xi_i = 2.0$. [Si/Fe] = 0.00, 0.20, 0.39 dex for the LTE line profiles, while [Si/Fe] = 0.00 for the NLTE calculation.

investigation of the *H*-band Si spectral lines. The NLTE corrections of strong lines range from -0.2 to -0.1 dex for giant stars in our sample. In extreme cases of APOGEE targets, the correction could be up to -0.4 dex. Thus they may have a significant impact on the Si abundances derived from APOGEE observations. Motivated by these results, the APOGEE team is planning to pursue more extended NLTE calculations in the coming years.

This research is supported by National Key Basic Research Program of China 2014CB845700, and by the National Natural Science Foundation of China under grant Nos. 11321064, 11233004, 11390371, 11473033, 11428308, U1331122. CAP is thankful to the Spanish MINECO for support through grant AYA2014-56359-P.

We acknowledge the support of the staff of the Xing-long 2.16m telescope. This work was partially Supported

by the Open Project Program of the Key Laboratory of Optical Astronomy, National Astronomical Observatories, Chinese Academy of Sciences. We thank Yoichi Takeda, Bun'ei Sato and Yujuan Liu for providing us the optical data. The authors thank the anonymous referee for comments that helped to improve the manuscript.

This research uses services or data provided by the NOAO Science Archive. NOAO is operated by the Association of Universities for Research in Astronomy (AURA), Inc. under a cooperative agreement with the National Science Foundation.

This work has made use of the VALD database, operated at Uppsala University, the Institute of Astronomy RAS in Moscow, and the University of Vienna.

Funding for SDSS-III has been provided by the Alfred P. Sloan Foundation, the Participating Institutions, the National Science Foundation, and the U.S. Department of Energy Office of Science. The SDSS-III web site is <http://www.sdss3.org/>.

SDSS-III is managed by the Astrophysical Research Consortium for the Participating Institutions of the SDSS-III Collaboration including the University of Arizona, the Brazilian Participation Group, Brookhaven National Laboratory, Carnegie Mellon University, University of Florida, the French Participation Group, the German Participation Group, Harvard University, the Instituto de Astrofísica de Canarias, the Michigan State/Notre Dame/JINA Participation Group, Johns Hopkins University, Lawrence Berkeley National Laboratory, Max Planck Institute for Astrophysics, Max Planck Institute for Extraterrestrial Physics, New Mexico State University, New York University, Ohio State University, Pennsylvania State University, University of Portsmouth, Princeton University, the Spanish Participation Group, University of Tokyo, University of Utah, Vanderbilt University, University of Virginia, University of Washington, and Yale University.

REFERENCES

- Ahn, C. P., Alexandroff, R., Allende Prieto, C., et al. 2014, *ApJS*, 211, 17
 Alam, S., Albareti, F. D., Allende Prieto, C., et al. 2015, *ApJS*, 219, 12
 Alonso, A., Arribas, S. & Martínez-Roger, C. 1996b, *A&A*, 313, 873
 Alonso, A., Arribas, S. & Martínez-Roger, C. 1999, *A&AS*, 140, 261
 Alonso, A., Arribas, S. & Martínez-Roger, C. 2001, *A&A*, 376, 1039
 Amarsi, A. M. & Asplund, M. 2016, *arXiv:1609.07283*
 Anstee, S. D. & O'Mara, B. J. 1991, *MNRAS*, 253, 549
 Anstee, S. D. & O'Mara, B. J. 1995, *MNRAS*, 276, 859

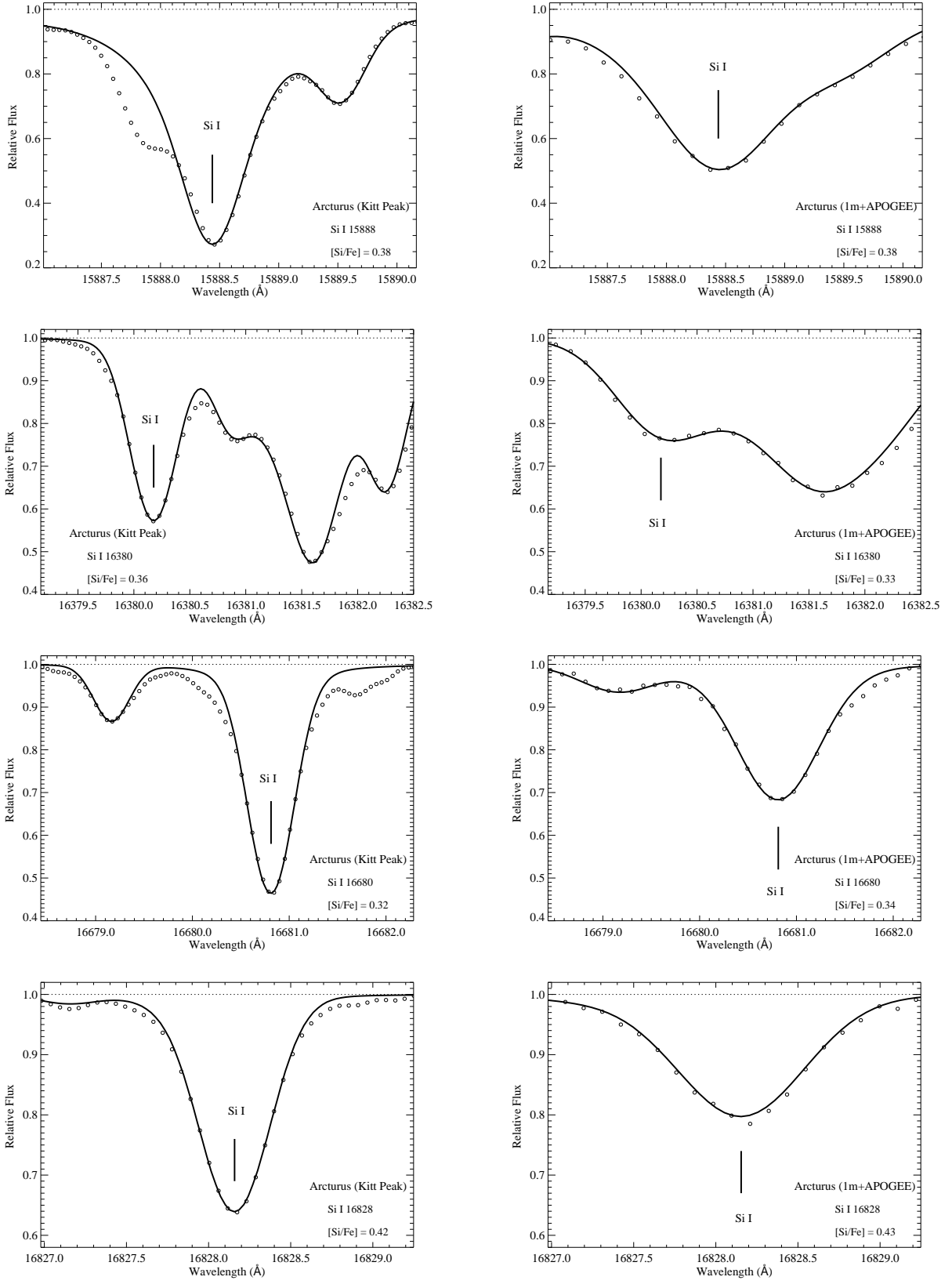


FIG. 8.— The NLTE best fitting profiles (solid lines) of the four investigated Si I lines in the Kitt Peak (Hinkle et al. 1995) and 1m+APOGEE observed spectra of Arcturus (open circles). The left panel for the spectrum of Arcturus from Hinkle et al. (1995) while the right panel for the 1m+APOGEE spectrum.

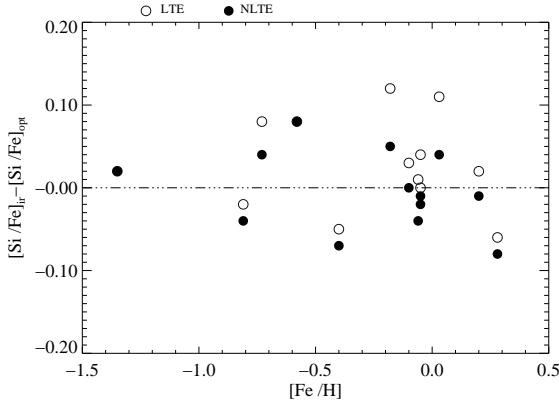


FIG. 9.— The difference between the mean Si abundances derived from IR and optical lines under LTE (open circles) and NLTE (filled circles) assumptions.

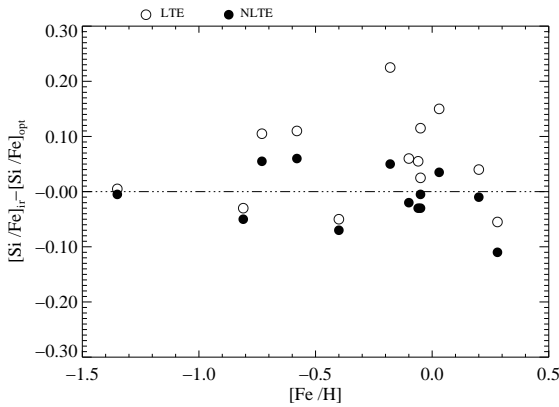


FIG. 10.— The difference between the Si abundances derived from the two strong Si I lines at 15888 and 16680 Å and the optical lines under LTE (open circles) and NLTE (filled circles).

Asplund, M., Grevesse, N., Sauval, A. J., et al. 2009, *ARA&A*, 47, 481
 Bard, A., & Kock, M. 1994, *A&A*, 282, 1014
 Bard, A., Kock, A., & Kock, M. 1991, *A&A*, 248, 315
 Barklem, P. S. & O'Mara, B. J. 1997, *MNRAS*, 290, 102
 Barklem, P. S., O'Mara, B. J., & Ross, J. E. 1998, *MNRAS*, 296, 1057
 Barklem, P. S., Piskunov, N., & O'Mara, B. J. 2000, *A&AS*, 142, 467
 Belyaev, A. K., Yakovleva, S. A., & Barklem, P. S. 2014, *A&A*, 572, A103
 Bensby, T., Feltzing, S., Lundström, I., et al. 2005, *A&A*, 433, 185
 Bensby, T., Feltzing, S., & Oey, M. S. 2014, *A&A*, 562, A71
 Bergemann, M., Kudritzki, R. P., Würl, M., et al. 2013, *ApJ*, 764, 115
 Blackwell, D. E., Shallis, M. J., & Simmons, G. J. 1980, *A&A*, 81, 340
 Butler, K. & Giddings, J. 1985, *Newsletter on the Analysis of Astronomical Spectra*, University of London, p. 9
 Eisenstein, D. J., Weinberg, D. H., Agol, E., et al. 2011, *AJ*, 142, 72
 Feuillet, D. K., Bovy, J., & Holtzman, J., et al. 2016, *ApJ*, 817, 40
 Fuhrmann, K. 1998, *A&A*, 338, 161
 Fuhr, J. R., Martin, G. A., & Wiese, W. L. 1988, *J. Phys. Chem. Ref. Data*, 17, Suppl. 4
 García Pérez, A. E., Allende Prieto, C., Holtzman, J. A., et al. 2016, *AJ*, 151, 144
 Garz, T. 1973, *A&A*, 26, 471

Gehren, T., Butler, K., Mashonkina, L., et al. 2001, *A&A*, 366, 981
 Goswami, A. & Prantzos, N. 2000, *A&A*, 359, 191
 Grevesse, N., Asplund, M., & Sauval, A. J. 2007, *Space Sci. Rev.*, 130, 105
 Gustafsson, B., Edvardsson, B., Eriksson, K., et al. 2008, *A&A*, 486, 951
 Hall, D. N. B., Ridgway, S. T., Bell, E. A., et al. 1979, *Proc. SPIE*, 172, 121
 Hawkins, K., Masseron, T., Jofre, P., et al. 2016, *arXiv:1604.08800*
 Henry, L., Vardya, M. S., & Bodenheimer, P. 1965, *ApJ*, 142, 841
 Hinkle, K., Wallace, L., & Livingston, W. 1995, *PASP*, 107, 1042
 Hinkle, K., Wallace, L., Valenti, J., et al. 2000, *Visible and Near Infrared Atlas of the Arcturus Spectrum 3727-9300 Å* (San Francisco: ASP)
 Hinkle, K. & Wallace, L. 2005, in *ASP Conf. Ser. 336, Cosmic Abundances as Records of Stellar Evolution and Nucleosynthesis*, ed. T.G. Barnes III & F.N. Bash (San Francisco, CA: ASP), 321
 Holtzman, J. A., Shetrone, M., Johnson, J. A., et al. 2015, *AJ*, 150, 148
 Holweber, H. 1973, *A&A*, 26, 275
 Izumiura, H. 2003, *Astronomical Herald*, 96, 291
 Johnson, T. V., Mousis, O., Lunine, J. I., & Madhusudhan, N., 2011, *LPI Contributions*, 1639, 9011
 Kamp, L. W. 1973, *ApJ*, 180, 447
 Kamp, L. W. 1978, *ApJ*, 36, 143
 Kamp, L. W. 1982, *ApJ*, 48, 415
 Kelleher, D. E. & Podobedova, L. I., 2008, *Journal of Physical and Chemical Reference Data*, 37, 1285
 Kobayashi, C., Karakas, A. I., & Umeda, H. 2011, *MNRAS*, 414, 3231
 Kurucz, R. L., Furenlid, I., Brault, J., et al. 1984, *Solar Flux Atlas from 296 to 1300 nm*, Kitt Peak National Solar Observatory
 Kurucz, R. L. 2007, Robert L. Kurucz online database of observed and predicted atomic transitions, <http://kurucz.harvard.edu>
 Kurucz, R. L. 2014, Robert L. Kurucz online database of observed and predicted atomic transitions, <http://kurucz.harvard.edu>
 Lee, Y. S., Beers, T. C., An, D., et al. 2011, *ApJ*, 738, 187
 Majewski, S. R., Schiavon, R. P., Allende Prieto, C., et al. 2015, *arXiv:1509.05420*
 Mashonkina, L., Korn, A. J. & Przybilla, N. 2007, *A&A*, 461, 261
 Mashonkina, L., Gehren, T., Shi, J. R., et al. 2011, *A&A*, 528, A87
 Meléndez, J. & Barbuy, B. 1999, *ApJS*, 124, 527
 Mészáros, S., Holtzman, J., García Pérez, A. E., et al. 2013, *AJ*, 146, 133
 Nahar, S. N. & Pradhan, A. K. 1993, *J. Phys. B*, 26, 1109
 Nidever, D. L., Holtzman, J. A., & Allende Prieto, C., et al. 2015, *AJ*, 150, 173
 Nissen, P. E. & Schuster, W. J. 2010, *A&A*, 511, L10
 O'Brien, T. R., Wickliffe, M. E., Lawler, J. E., et al. 1991, *J. Opt. Soc. Am. B*, 8, 1185
 Pfeiffer, M. J., Frank, C., Baumüller, D. et al. 1998, *A&AS*, 130, 381
 Ramírez, I. & Allende Prieto, C. 2011, *ApJ*, 743, 135
 Reddy, B. E., Tomkin, J., Lambert, D. L., et al. 2003, *MNRAS*, 340, 304
 Reddy, B. E., Lambert, D. L. & Allende Prieto, C. 2006, *MNRAS*, 367, 1329
 Reetz, J. K. 1991, *Diploma thesis*, Universität München
 Romano, D., Karakas, A. I., Tosi, M. et al. 2010, *A&A*, 522, A32
 Ryabchikova, T. A., Piskunov, N. E., Stempels, H. C. et al. 1999, *Physica Scripta Volume T*, 83, 162
 Rybicki, G. B. & Hummer, D. G. 1991, *A&A*, 245, 171
 Rybicki, G. B. & Hummer, D. G. 1992, *A&A*, 262, 209
 Samland, M. 1998, *ApJ*, 496, 155
 Sheminova, V. A. 2015, *Kinematics and Physics of Celestial Bodies*, 31, 172
 Shi, J. R., Gehren, T., Butler, K., et al. 2008, *A&A*, 486, 303
 Shi, J. R., Gehren, T., Mashonkina, L., et al. 2009, *A&A*, 503, 533
 Shi, J. R., Gehren, T. & Zhao, G. 2011, *A&A*, 534, A103
 Shi, J. R., Takada-Hidai, M., Takeda, Y., et al. 2012, *ApJ*, 755, 36
 Takeda, Y., Sato, B. & Murata, D. 2008, *PASJ*, 60, 781
 Tsujimoto, T., Nomoto, K., Yoshii, Y., et al. 1995, *MNRAS*, 277, 945
 Wang, X. M., Shi, J. R. & Zhao, G. 2009, *MNRAS*, 399, 1264
 Wedemeyer, S. 2001, *A&A*, 2001, 373, 998
 Woosley, S. E. & Weaver, T. A. 1995, *ApJS*, 101, 181
 Wilson, J. C., Hearty, F., Skrutskie, M. F., et al. 2010, *Proc. SPIE*, 7735
 Zambardi, T., Poitras, F., Corgne, A., et al. 2013, *Geochim. Cosmochim. Acta*, 121, 67
 Zhang, L., Karlsson, T., Christlieb, N., et al. 2011, *A&A*, 528, A92
 Zhao, G. & Li, H. B. 2001, *Chinese J. Astron. Astrophys.*, 1, 555

APPENDIX

TABLE 6
LINE DATA, IRON ABUNDANCES DERIVED FROM THE SOLAR SPECTRUM AND
EQUIVALENT WIDTHS OF THE SOLAR LINES

λ (Å)	χ (eV)	$\log C_6$	$\log gf$	Ref.	$\log \varepsilon_{\odot} \text{Fe}$ LTE (dex)	$\log \varepsilon_{\odot} \text{Fe}$ NLTE (dex)	$\log gf'$	EW (mÅ)
Fe I								
4661.534	4.558	-29.481	-1.27	FUH88	7.57	7.61	-1.16	40.5
4808.149	3.251	-31.464	-2.79	FUH88	7.66	7.70	-2.59	29.5
4885.430	3.882	-30.173	-1.02	KUR14	7.49	7.55	-0.97	91.3
5223.186	3.635	-31.165	-1.78	BRI91	7.05	7.09	-2.19	31.0
5242.497	3.634	-31.248	-0.97	BRI91	7.56	7.52	-0.95	90.3
5379.579	4.154	-31.242	-1.51	BRI91	7.57	7.57	-1.44	63.5
5398.279	4.371	-30.155	-0.67	FUH88	7.55	7.59	-0.58	78.8
5522.449	4.217	-30.457	-1.55	FUH88	7.63	7.68	-1.37	44.9
5546.506	4.434	-30.356	-1.31	FUH88	7.68	7.74	-1.07	52.7
5618.633	4.386	-30.475	-1.28	BRI91	7.49	7.55	-1.23	52.2
5651.469	4.386	-30.264	-2.00	FUH88	7.77	7.78	-1.72	19.5
5679.023	4.186	-30.040	-0.92	FUH88	7.72	7.78	-0.64	65.0
5793.915	4.220	-30.505	-1.70	FUH88	7.58	7.63	-1.57	35.5
5853.148	1.485	-31.586	-5.28	FUH88	7.64	7.67	-5.11	8.1
5855.077	4.608	-30.189	-1.48	BAR94	7.43	7.48	-1.50	23.3
5929.677	4.548	-30.305	-1.41	FUH88	7.71	7.77	-1.14	41.7
6024.058	4.548	-30.358	-0.12	FUH88	7.66	7.70	0.08	127.5
6078.491	4.796	-29.749	-0.32	KUR14	7.47	7.52	-0.30	84.6
6079.009	4.652	-30.237	-1.12	FUH88	7.64	7.70	-0.92	48.8
6151.623	2.176	-31.538	-3.30	FUH88	7.53	7.55	-3.25	51.6
6173.335	2.223	-31.523	-2.88	FUH88	7.56	7.58	-2.80	70.1
6200.321	2.608	-31.279	-2.44	FUH88	7.59	7.59	-2.35	75.2
6240.646	2.223	-31.450	-3.23	BAR91	7.44	7.46	-3.27	48.7
6322.686	2.588	-31.296	-2.43	FUH88	7.60	7.60	-2.33	77.6
6335.331	2.198	-31.546	-2.18	BRI91	7.46	7.46	-2.22	103.3
6481.877	2.279	-31.420	-2.98	FUH88	7.58	7.60	-2.88	65.7
6593.871	2.433	-31.375	-2.42	FUH88	7.62	7.63	-2.29	98.7
6726.666	4.607	-30.256	-1.09	KUR14	7.56	7.63	-0.96	50.2
6839.831	2.559	-31.346	-3.45	FUH88	7.55	7.58	-3.37	30.3
6857.250	4.076	-30.895	-2.15	FUH88	7.56	7.61	-2.04	23.4
mean					7.56	7.60		
σ					0.13	0.13		
Fe II								
4508.288	2.856	-31.971	-2.25	RYA99	7.48	7.48	-2.27	77.6
5264.808	3.230	-31.977	-3.12	RYA99	7.53	7.53	-3.09	103.3
5414.073	3.221	-31.976	-3.54	RYA99	7.45	7.45	-3.60	65.7
5991.376	3.153	-31.983	-3.54	BLA80	7.43	7.43	-3.61	98.7
6149.258	3.889	-32.048	-2.72	BLA80	7.49	7.49	-2.73	50.2
6456.383	3.903	-31.979	-2.10	BLA80	7.54	7.54	-2.07	30.3
mean					7.49	7.49		
σ					0.04	0.04		

NOTE. — References to the $\log gf$ values are FUH88: Fuhr et al. (1988), KUR14: Kurucz (2014), BRI91: O'Brien et al. (1991), BAR94: Bard & Kock (1994), BAR91: Bard et al. (1991), RYA99: Ryabchikova et al. (1999) and BLA80: Blackwell et al. (1980). The $\log C_6$ values were calculated according to Anstee & O'Mara (1991, 1995) and Barklem et al. (2000). σ refers to the statistical error. The $\log gf'$ denotes that the gf -values were derived from the NLTE solar fits.

TABLE 7
SILICON RELATIVE TO IRON ABUNDANCES BASED ON OPTICAL Si I LINES UNDER LTE AND NLTE ANALYSES

Star	5701 (Å)		5772 (Å)		6142 (Å)		6145 (Å)		6155 (Å)		6237 (Å)		6243 (Å)		6244 (Å)	
	LTE	NLTE	LTE	NLTE	LTE	NLTE	LTE	NLTE	LTE	NLTE	LTE	NLTE	LTE	NLTE	LTE	NLTE
Arcturus	0.32	0.27			0.31	0.28			0.38	0.28	0.36	0.30	0.36	0.32		
HD 87	0.15	0.12	0.19	0.13	0.12	0.11	0.14	0.13	0.13	0.13						
HD 6582	0.27	0.27	0.27	0.26			0.27	0.27	0.26	0.25	0.23	0.23	0.31	0.31	0.27	0.27
HD 6920			0.06	0.03			0.00	-0.01	0.10	0.05						
HD 22675	0.11	0.08	0.14	0.07	0.07	0.05	0.08	0.06	0.17	0.10						
HD 31501	0.21	0.20			0.18	0.18	0.23	0.22	0.22	0.20			0.25	0.24	0.22	0.21
HD 58367	0.15	0.11			0.11	0.11	0.13	0.13	0.23	0.15						
HD 67447	0.11	0.07	0.15	0.08	0.06	0.05	0.10	0.09	0.17	0.08	0.15	0.10	0.08	0.06	0.13	0.09
HD 102870	-0.09	-0.10	-0.05	-0.07	-0.08	-0.08	-0.06	-0.06	-0.03	-0.05	-0.09	-0.10	-0.07	-0.07	-0.09	-0.09
HD 103095	0.36	0.35							0.25	0.25	0.30	0.30	0.32	0.32	0.28	0.28
HD 121370			0.21	0.18	0.17	0.17	0.17	0.17	0.29	0.23	0.24	0.21				
HD 148816			0.18	0.17	0.14	0.14	0.23	0.23	0.17	0.16	0.17	0.17	0.18	0.18	0.19	0.19
HD 177249	0.04	0.02			0.05	0.05	0.02	0.02	0.13	0.07						

TABLE 8
EQUIVALENT WIDTHS OF NEUTRAL IRON LINES FOR SAMPLE STARS.

λ (Å)	Arcturus	HD 87	HD 6582	HD 6920	HD 22675	HD 31501	HD 58367	HD 67447	HD 102870	HD 103095	HD 121370	HD 148816	HD 177249
4661.534	---	---	18.0	39.8	---	---	---	89.5	40.4	8.0	48.7	10.4	---
4808.149	---	---	11.5	25.6	---	---	---	72.4	28.8	8.4	37.1	7.1	---
4885.430	---	---	55.7	75.3	---	---	---	126.2	77.8	38.1	87.9	37.7	---
5223.186	64.3	52.0	14.7	32.5	61.5	---	---	67.8	30.7	8.7	37.3	7.2	---
5242.497	117.5	115.9	63.6	92.2	120.9	---	146.5	146.4	92.0	54.9	108.0	54.8	121.6
5379.579	90.9	87.5	38.1	59.5	93.8	---	111.4	114.7	63.7	22.4	76.1	27.7	93.4
5398.279	91.1	94.7	48.3	71.0	104.2	---	116.8	124.5	78.9	33.2	88.7	38.5	102.9
5522.449	61.0	66.2	20.1	41.5	71.1	---	78.8	84.3	44.1	10.6	57.0	14.3	69.8
5546.506	72.2	75.1	26.0	51.0	81.7	---	91.6	100.4	53.4	14.1	68.8	17.7	80.4
5618.633	71.0	69.4	27.4	50.3	76.0	42.3	88.9	93.6	53.2	12.3	65.3	18.4	77.6
5651.469	32.2	33.5	6.6	18.8	39.7	14.6	45.7	45.1	19.2	---	27.3	---	35.8
5679.023	70.0	76.4	32.8	61.2	81.9	53.7	87.9	97.2	60.8	17.1	72.0	24.0	81.5
5793.915	53.6	58.6	12.9	29.8	62.1	28.1	70.0	84.6	34.4	6.1	45.9	9.3	72.0
5853.148	---	---	---	---	44.2	12.0	45.1	51.5	6.0	---	10.5	---	27.4
5855.077	34.2	39.9	7.8	22.0	43.9	17.5	---	49.5	23.0	---	31.2	5.3	39.2
5929.677	54.7	63.3	16.3	---	67.6	37.7	73.9	78.0	40.4	17.0	50.9	17.0	63.4
6024.058	116.8	125.7	87.0	107.5	132.6	120.1	---	156.0	114.0	70.3	124.7	66.7	135.0
6078.491	81.2	93.8	47.5	76.6	99.0	81.2	---	117.0	82.5	29.5	92.8	35.2	99.2
6079.009	58.3	62.9	19.3	40.7	69.7	41.6	80.0	85.4	48.9	9.2	54.2	13.7	70.1
6151.623	114.6	88.1	31.3	47.5	97.9	51.4	117.4	122.1	45.4	21.4	54.7	17.4	91.5
6173.335	133.0	109.5	48.3	70.3	119.9	52.3	146.8	148.9	66.0	40.0	78.0	33.7	115.1
6200.321	132.7	111.0	52.2	73.0	121.7	74.2	140.3	148.0	78.8	41.4	87.1	34.5	116.4
6240.646	114.7	---	29.8	43.7	---	52.3	---	127.4	43.2	19.8	55.2	16.5	---
6322.686	140.7	---	53.8	76.8	---	76.7	---	150.6	73.0	44.3	91.0	40.6	---
6335.331	132.6	---	85.1	103.5	---	109.1	---	196.0	98.4	79.2	115.3	66.2	---
6481.877	---	---	---	63.9	---	72.4	---	142.9	62.4	34.1	76.6	27.5	---
6593.871	---	---	68.8	89.1	---	90.6	---	177.7	93.9	61.3	101.1	55.4	---
6726.666	---	---	19.8	50.0	---	42.1	---	86.6	49.6	9.8	62.8	15.3	---
6839.831	---	---	15.3	---	---	32.2	---	94.5	28.9	8.2	43.5	7.2	---
6857.250	---	---	---	---	---	18.8	---	55.3	---	---	---	5.9	---

NOTE. — Seriously blending lines and the lines with bad S/N are rejected during determining the stellar parameters for a given star.